Research Article

Khadija Rafique*, Zafar Mahmood*, Adnan, Umar Khan, Bilal Ali, Fuad A. Awwad, and Emad A. A. Ismail

Numerical analysis of non-linear radiative Casson fluids containing CNTs having length and radius over permeable moving plate

https://doi.org/10.1515/phys-2024-0013
received December 26, 2023; accepted March 20, 2024

Abstract: Casson fluids containing carbon nanotubes of various lengths and radii on a moving permeable plate reduce friction and improve equipment efficiency. They improve plate flow dynamics to improve heat transfer, particularly in electronic cooling and heat exchangers. The core objective of this study is to investigate the heat transmission mechanism and identify the prerequisites for achieving high cooling speeds within a two-dimensional, stable, axisymmetric boundary layer. This study considers a sodium alginate-based nanofluid containing single/multi-wall carbon nanotubes (SWCNTs/MWCNTs) and Casson nanofluid flow on a permeable moving plate with varying length, radius, and nonlinear thermal radiation effects. The plate has the capacity to move either parallel to or perpendicular to the free stream. The governing partial differential equations for the boundary layer, which are interconnected, are transformed into standard differential equations. These equations are then numerically solved using the Runge–Kutta fourth-order scheme incorporated in the shooting method. This research analyses and graphically displays the effects of factors including mass suction, nanoparticle volume fraction, Casson parameter, thermal radiation, and temperature ratio. Additionally, a comparison is made between the present result and the previous finding, which presented in a tabular format. The coefficient of skin friction decreases in correlation with an increase in Casson fluid parameters and Prandtl number. Heat transfer rate decreases with a variation in viscosity parameter, while it is increasing with an increase in Prandtl number. In addition, this study demonstrates that heat transfer rate for MWCNT is significantly higher than that of SWCNT nanoparticles. Thermal radiation and temperature ratio reduce the heat transfer rate, whereas nanoparticle volume fraction and Casson parameter enhance it over a shrinking surface.

Keywords: Yamada–Ota model, CNTs, nonlinear thermal radiation, mass suction, numerical analysis

*** Corresponding author: Khadija Rafique,** Department of Mathematics and Statistics, Hazara University, Mansehra 21300, Pakistan, e-mail: khadijarafique101@gmail.com
*** Corresponding author: Zafar Mahmood,** Department of Mathematics and Statistics, Hazara University, Mansehra 21300, Pakistan, e-mail: zafarmaths222@gmail.com
Adnan: Department of Mathematics, Mohi-ud-Din Islamic University, Nerian Sharif, AJ&K, Pakistan
Umar Khan: Department of Mathematics and Statistics, Hazara University, Mansehra 21300, Pakistan
Bilal Ali: School of Mathematics and Statistics, Central South University, Changsha 410083, China
Fuad A. Awwad, Emad A. A. Ismail: Department of Quantitative Analysis, College of Business Administration, King Saud University, P.O. Box 71115, Riyadh 11587, Saudi Arabia

Nomenclature

x, y	Cartesian coordinates
a, b	constants
u, v	velocity component along the x- and y-axis (m s^{-1})
u_e	free stream velocity (m s^{-1})
(ρC_p)	fluid's heat capacitance (J K^{-1} m^{-3})
C_f	skin friction
$q_{\bar{w}}$	heat flux
M	magnetic parameter
C_p	specific heat capacitance (J kg^{-1} K^{-1})
Nu_x	Nusselt number
k^*	thermal conductivity (W m^{-1} K^{-1})
θ	dimensionless temperature
η	similarity variables
Pr	Prandtl number
q_w	surface heat flux
λ	shrinking parameter
β	Casson parameter
Re_x	local Reynold number
θ_w	temperature ratio parameter
Rd	radiation parameter

Open Access. © 2024 the author(s), published by De Gruyter. This work is licensed under the Creative Commons Attribution 4.0 International License.

t	time (s)
T	temperature (K)
T_w	constant surface temperature (K)
K_{CNT}	thermal conductivity of carbon nanotube
ρ_{CNT}	density of carbon nanotubes
T_∞	ambient temperature (K)
u_w	mass suction velocity (m s^{-1})
$S > 0$	suction
$S < 0$	infection
v_w	surface velocity (m s^{-1})
ν	kinematic viscosity (m^2 s^{-1})
ρ	density (kg m^{-3})
ϕ	nanoparticle volume fraction (%)
$\tau_{\tilde{w}x}$	heat capacity ratio
Ω	viscosity parameter

Subscripts

f	base fluid
nf	nanofluid

Acronyms

ODEs	ordinary differential equations
RKF	Runge–Kutta–Fehlberg

1 Introduction

Non-Newtonian fluids have generated a significant amount of interest because of the several technological and industrial domains in which they have the potential to provide applications. They are used, for instance, in the production of polymers, pharmaceuticals made from syrups, and crude oil from petroleum derivatives. In a work that was carried out by Hamid and colleagues [1], the effects of Casson nanofluid on a surface that is malleable were investigated. Jamshed and colleagues [2] conducted another study that specifically observed into the effects of Casson nanofluid flow. The work of Gomathi and De [3] looked into how hall currents and ion slip affect the flow of a mixed Casson Williamson nanofluid with viscous dissipation across a porous media. The work of Poulomi and Ekambaram [4] looked at the bioconvective Casson nanofluid flow in the direction of the stagnation point using a non-Darcy porous medium that had buoyancy effects and heat radiation. Vinodkumar Reddy *et al.* [5] examined the convective maximum hydrodynamic drag (MHD) stagnation point flow of a Casson nanofluid across a porous medium undergoing a chemical reaction with a heat source and Joule heating. A study conducted by Awan and colleagues [6] examined how MHD and the Darcy–Forchheimer law impact the behavior of a Casson–Sutterby nanofluid in an extended circular cylinder. Abbas *et al.* [7] used computational models to examine the flow of a hybrid nanofluid including MHD nonlinear radiation and Casson at a vertical stretching sheet. Lanjwani *et al.* [8] conducted an investigation on triple Casson nanofluid solutions on a sheet that underwent exponential vertical stretching and contraction. Cross-diffusion and heat source effects were investigated by Reddy and Lakshminarayana in relation to three-dimensional MHD Maxwell nanofluid flow across a stretched surface using chemical reactions [9]. Several authors have also contributed to the understanding of Casson fluid in various flow scenarios, as indicated by previous studies [10–14]. Nanofluids are used in a variety of industrial and nanotechnology-based activities, including the cooling systems of electronic gadgets, nuclear reactors, and other operations. Moreover, magnetic nanofluids prove beneficial in a wide range of uses, such as cancer therapy, facilitating wound recovery, clearing blocked arteries, and enhancing magnetic resonance imaging procedures, among others. As mentioned by Maleki *et al.* [15], pseudoplastic nanofluid influences the permeable stretching sheet when heat generation and viscous dissipation are present. Alazwari *et al.* [16] conducted an examination of the nanofluid's non-Newtonian fluid flow on stretched sheets. A few writers have studied nanofluids under exponential stretching recently [17].

Carbon nanotubes (CNTs) exhibit a cylindrical shape, with diameters typically falling within the range of 0.5–1.5 nm. These nanotubes, also referred to as graphene sheets, are highly acknowledged for their exceptional nanoparticle properties, primarily owing to their tubular structure that comprises carbon atoms. These nanotubes consist of a solitary layer of graphene constituents, where every atom is situated in a singular position. CNTs, including multi-wall carbon nanotubes (MWCNTs), surpass other nanoparticles and nanotubes in terms of mechanical and thermal properties, exhibiting superiority that is six times greater. The utilization of CNTs offers substantial benefits such as biomedical applications, wastewater treatment, and petrochemical facilities. Xue [18] conducted research that encompassed both experimental and theoretical studies of CNTs. Shahzad *et al.* [19] enhanced the heat transfer rate in solar collectors by using the Oldroyd-B model hybrid nanofluid along with a kerosene oil flow incorporating CNTs. In their study [20], Shamshuddin and colleagues investigated the dynamics of MWCNT and single-wall

carbon nanotubes (SWCNTs) using Joule heating and thermal radiation. Considering thermo-diffusion and chemical reactions, Kiran Kumar *et al.* [21] studied the effect of thermal radiation on the convective heat and mass transfer flow of water–SWCNT and MWCNT nanofluids in a cylindrical annulus. Hayat *et al.* [22] investigated the flow behavior of water-based CNTs carbon using the Darcy–Forchheimer model, specifically focusing on a convectively heated rotating disk. Their results revealed that as percentage of CNTs in the fluid volume increases, the fluid's velocity limitation also increases. The Yamada–Ota model provides an explanation for flow dynamics in multiphase systems in fluid mechanics. The field of computational fluid dynamics (CFD) can provide more accurate predictions of turbulent multiphase flows that include dispersed particles or droplets in a continuous fluid. Dispersed phase particles or droplets affect flow dynamics; hence, the Yamada–Ota model includes auxiliary equations. These equations include drag forces, turbulence dispersion, and interfacial momentum transfer between the dispersed and continuous phases. Several authors have also contributed to the understanding of fluid in various flow scenarios by considering the Yamada–Ota model [23,24].

Thermal radiation involves the release of heat energy from a surface as electromagnetic waves, propagating in all directions. This mechanism serves as the sole method of heat transfer in a vacuum and plays a significant role in generating high temperatures. In engineering and physics, thermal radiation is of paramount importance in heat transfer and fluid flow analyses involving diverse liquids. Moreover, the impact of thermal radiation holds great significance in space technology, particularly for devices operating under extremely high-temperature conditions. Recent studies have focused on examining the influence of thermal radiation. Imtiaz *et al.* [25] published a study examining Williamson fluid with suspended particles flow over a stretched surface while accounting for the nonlinear influence of heat radiation. The calculation of the power-law flow of nanofluids is dependent on temperature and occurs over a wide range of stretching. The Riga sheet was developed by Abbas *et al.* [26]. Mulinti and Lakshminarayana [27] explored how thermal radiation and viscous dissipation affect the MHD of a fluid moving over a porous stretched sheet with increasing chemical interactions. In their investigation, Khan *et al.* [28] looked at the effects of nonlinear radiation on the MHD flow of Carreau nanofluid across a surface that had been heated convectively. Additionally, Rehman *et al.* [29] focused on studying the combined impacts of thermal stratification and radiation on the flow of tangent hyperbolic fluid around a flat surface and a cylindrical surface. The study by Vinodkumar Reddy and Lakshminarayana [30] looked at how radiation affects the flow of a magnetohydrodynamic nanofluid over a stretched sheet in a porous medium. In a separate numerical enquiry by Mushtaq *et al.* [31], the flow of nanofluids driven by solar energy was examined, with special consideration given to the effects of nonlinear thermal radiation. Rehman and Eltayeb [32] examined the characteristics of hydromagnetic nanofluids flowing over a nonlinear stretched surface, considering convective boundary conditions and thermal radiation. Sheikholeslami *et al.* [33] did their own research project in which they looked into how thermal radiation affects the flow of MHD nanofluids between two plates that are moving horizontally while magnetic fields are present. Turkyilmazoglu and Pop [34] focused on the investigation of mass and heat transport properties of nanofluids as they flow over a vertically infinite flat plate subjected to heating.

Sakiadis [35] was first to scrutinize the boundary layer's behavior on a continuously solid surface. He noted a striking difference between the behavior of the respected surface and boundary layer of a fluid traveling over a flat, stable, smooth surface as studied by Blasius [36]. In a similar vein, Tsou *et al.* [37] conducted an experimental and theoretical investigation. Their study yielded a notable finding that observed laminar velocity field aligned precisely with analytical predictions, thus confirming their agreement. Tsai and Hsu [38] investigated the thermal transfer characteristics in a non-Newtonian fluid. Their research revealed that the power law index, denoted as "n," and the generalized Prandtl number significantly influenced both the flow and heat fields. When thermal radiation occurs, Cortell Bataller [39] looked at how the Prandtl number affects the lowering of a plate's thermal border thickness within the framework of classical Blasius flow. Haile and Shankar [40] emphasized the importance of chemical processes, viscosity dispersion, and heat radiation throughout their work. In their investigation, various factors including viscous dissipation and thermal radiation were found to elevate temperature profile, while the Prandtl number and velocity parameter exhibited significant decreases. Additionally, when compared to the other characteristics that were evaluated, the thermophoresis parameter had a significantly different impact on the concentration profile than the other parameters. Awan *et al.* [41] carried out a theoretical examination of unstable oblique stagnation point-based Jeffrey nanofluid flow by making use of an oscillating stretching sheet.

The demand for smaller electronic components and devices is expected to continue to climb, which will result in an increased demand for fluids that have improved heat conductivity. Engineers and researchers created a special fluid known as nanofluid to address this issue. Nanofluid is made up of particles that are so minute that they can be

measured in micromillimeters. These particles are distributed throughout the typical mediums that are used for heat transfer. It is anticipated that the higher thermal conductivity of nanofluids will surpass that of normal fluids, which will result in an improvement in the efficiency with which heat is effectively transmitted. Because of this, the efficiency of heat transport would increase. When solid nanoparticles were combined with a base fluid, the term "nanofluid" was initially developed to characterize the combination of these nanoparticles. Choi should be credited as the only creator of the word. Following the initial hypothesis, subsequent studies demonstrated that nanoparticles have the capacity to improve heat conductivity, hence providing support for the theory. Researchers have conducted an exhaustive investigation to explore the characteristics and possessions of nanofluids in a variety of different environments. The stagnation point flow, parallel rotating plates, microchannels, and cylindrical geometries are all included in these settings. A great number of experiments have been carried out to bring attention to the novel characteristics of nanofluids and to study the possible applications that could be associated with these fluids. Numerous researchers have conducted research on the topic of nanofluids, as shown by previous studies [42–44].

To accurately assess the positive effect an influence has had on the flow, one must consider all of the many factors influencing the flow. The suction phenomenon, which is crucial for the boundary-layer management, has been the subject of much investigation. Dipping friction in external flows and minimizing energy loss in channels are two instances of the phenomena. Minimizing energy loss in channels is another illustration of this. Both issues will be discussed in greater detail later. As an illustration of an efficient method to impede or postpone the separation of the boundary layer, this serves as an example. When trying to induce a suction effect, surface modification is necessary. Openings such as holes, gaps, porous patches, or perforations can be incorporated into the structure to accomplish this goal. The integration of these channels makes it possible to extract the boundary-layer component that has the slowest flow rate and is in the closest vicinity to the wall. One of the consequences of this is that it improves the uniformity and stability of the velocity profile within the boundary layer, which ultimately leads to a reduction in the chance of the boundary-layer separation. In a study by Alqahtani *et al.* [45], the results show that controlling the boundary-layer well depends on both the sticking together of nanoparticles and the changing of viscosity. Preventing boundary-layer separation as quickly as possible is frequently essential for generating higher lift coefficients and reducing the amount of drag that an aircraft experiences. Utilizing the Galerkin finite element approach, Al-Kouz *et al.* [46] investigated heat transfer and entropy formation in a CNT hybrid magnetic nanofluid flow inside a trapezoidal wavy enclosure that included porous media. Researchers of exceptional caliber, such as Masad *et al.* [47], Rosali *et al.* [48], and Pandey and Kumar [49], have investigated the influence that suction has on a wide variety of surface types and fluid properties. Research into non-linear radiative Casson fluids containing CNTs and flow across a permeable surface is an activity that involves several disciplines and has far-reaching effects. There are several disciplines that may benefit from it, including engineering, physics, biology, and materials science. This study provides significant contributions to the understanding of fluid behavior in complex systems, thereby facilitating the development of technologies that exhibit enhanced performance and efficiency. Changing viscosity in Casson fluids with CNTs of a certain length and radius flowing through a moveable permeable plate is an interesting topic for scientific investigation. More research in this area could help us better comprehend complicated fluid dynamics. For a wide variety of engineering uses, it will also improve the accuracy of prediction models and the efficiency of related technologies. Studying the impact of CNT length and radius on fluid viscosity can provide valuable insights. These findings may improve nanofluid-based systems, particularly heat exchangers, biomedical devices, and nanofluidic devices, where design and performance are paramount. Many important scientific and engineering fields are interested in studying Casson fluids, which are made up of CNTs of a certain length and radius moving across a permeable moving plate. It is vital to underline numerous crucial variables to emphasize the significance of this research. Casson viscosity and yield stress are two of the most important factors that play a significant part in determining the non-Newtonian features that Casson fluids exhibit. The insertion of CNTs of a particular length and radius can change the rheological properties of the fluid, which will therefore influence the flow and deformation features of the fluid. Within the context of applications that need precise control of fluid behavior, it becomes very necessary to have a comprehensive understanding of these modifications. When it comes to applications that are associated with heat transmission, it is vital to examine the impact of radiative effects in the context of Casson fluids that contain CNTs. Even though CNTs are well known for their thermal conductivity, the simple existence of these particles has the potential to influence the heat transfer capabilities of the fluid. This comprehension is necessary for the development of technologies and applications in a wide range of domains, such as the science of materials, nanotechnology, heat transfer, and fluid

dynamics, among others. To best of authors' knowledge, no previous studies have been carried out on flow of Casson nanofluid, which contains SWCNTs and MWCNTs, over a permeable moving sheet while considering the effects of non-linear radiation, varying Prandtl number, and variable viscosity. The authors chose the moving plate arrangement despite substantial research on non-Newtonian fluids in a variety of geometries due to the expanding industrial application of non-Newtonian fluids. MHD generators, gas turbines, and plastic sheet extrusion all significantly depend on flow of such fluids over a permeable moving sheet. The shooting method and Runge–Kutta fourth-order (RK-IV) were coupled to find the problem's numerical solution. The key questions of the current study are as follows:

- How the thermal performance of working fluid can be improved?
- How does a viscosity that changes as a function of temperature affect the relationship between velocity and temperature profile?
- How will velocity and temperature profile behave with impact of varying Prandtl number?
- How radiation and variable Prandtl number parameter influence the heat transfer rate?

2 Problem statement

In this work, the analysis of the stable and axisymmetric boundary layer of a Casson nanofluid is the primary focus of attention. The nanofluid under consideration contains CNTs with both single and multiple walls. This flow takes place in a uniform free stream that is designated by u_e and happens over a permeable plate. It is presumed that the nanofluid is in a state of thermal equilibrium and that it is adhering to conditions that prevent it from sliding. The fluid motion is confined to the region where x and y with the axis aligned parallel to the surface of the plate and the y-axis perpendicular to it. The temperature of the plate, T, is maintained at a constant value of T_w, while the surrounding fluid's temperature is denoted as T_∞. The velocity of shrinking plate is u_w. Additionally, the study considers the influence of suction, denoted as S, as depicted in Figure 1. The chosen base fluid for the nanoparticles is sodium alginate. Furthermore, the impact of variable viscosity, variable Prandtl number, and nonlinear thermal radiation is also considered. It is assumed that nanoparticles possess a uniform spherical shape and size. The thermophysical properties of the suspended nanofluid containing CNTs (SWCNTs and MWCNTs) are provided in Table 1.

By referencing the previous readings [50,51], we have developed the steady-flow-governing equations for the given problem geometry:

$$\frac{\partial u}{\partial x} + \frac{\partial v}{\partial y} = 0, \tag{1}$$

$$u\frac{\partial u}{\partial x} + v\frac{\partial u}{\partial y} = u_e\frac{\partial u_e}{\partial x} + \frac{1}{\rho_{nf}}\left(1 + \frac{1}{\beta}\right)\frac{\partial}{\partial y}\left[\mu_{nf}(T)\frac{\partial u}{\partial y}\right], \tag{2}$$

$$u\frac{\partial T}{\partial x} + v\frac{\partial T}{\partial y} = \frac{k_{CNT}}{(\rho C_p)_{CNT}}\frac{\partial^2 T}{\partial y^2} - \frac{1}{(\rho C_p)_{CNT}}\left(\frac{\partial q_r}{\partial y}\right). \tag{3}$$

Additionally, the symbols u and v are used to denote the velocity components along x- and y-axis, respectively. To provide a description of the radiative heat flow within the energy equation, the Roseland approximation is used. The

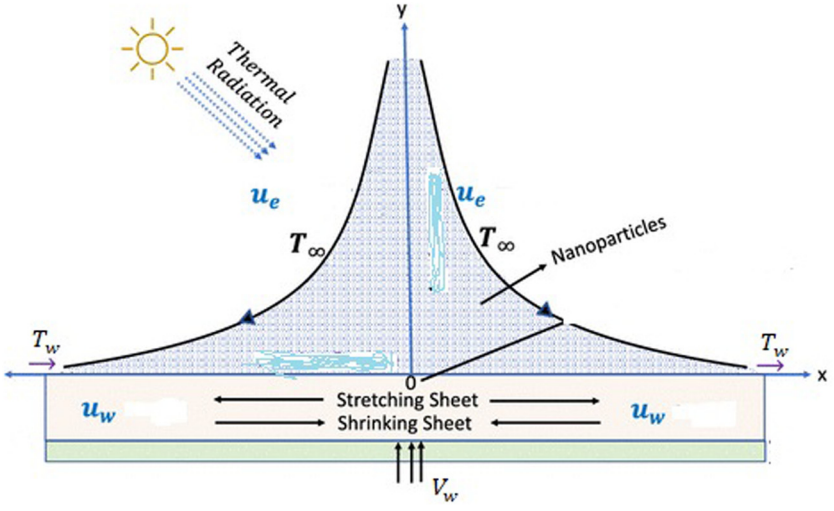

Figure 1: Overview of the issue conceptually.

Table 1: Thermophysical characteristics for various CNTS using base fluid [23,24]

Properties	MWCNT	SWCNT	Sodium alginate (SA)
ρ (kg/m^3)	1,600	2,600	989
k (W/m K)	3,000	6,600	0.6376
C_p (J/kg K)	796	425	4,175

formula for the term "thermal radiation" has been proposed by Rafique *et al.* [52].

$$q_r = -\frac{16\sigma^* T^3}{3k^*}\frac{\partial T}{\partial y}. \tag{4}$$

The coefficient of mean absorption is denoted by k^*, and the Stefan–Boltzmann constant is denoted by σ^* in this context. By adding Eqs. (4) and (3), the energy equation can be generalized as follows:

$$u\frac{\partial T}{\partial x} + v\frac{\partial T}{\partial y} = \frac{k_{CNT}}{(\rho C_p)_{CNT}}\frac{\partial^2 T}{\partial y^2} + \frac{1}{(\rho C_p)_{CNT}}\frac{16\sigma^*}{3k^*}\frac{\partial}{\partial y}\left(T^3\frac{\partial T}{\partial y}\right). \tag{5}$$

Subsequently, pertaining to the subsequent set of boundary conditions (BCs), see reference [50]:

$$u = u_w = ax, v = V_w = \left(\frac{u_e\nu_f}{2x}\right)^{\frac{1}{2}} S, T = T_w, \quad \text{at} \quad y = 0,$$
$$u \to u_e = bx, T \to T_\infty, \quad \text{as} \quad y \to \infty. \tag{6}$$

The temperature of the nanofluid containing CNT is meant by T, temperature-dependent variable viscosity is $\mu_{nf}(T) = \mu_{nf}(T)[1 + \xi(T_w - T)]$, where ξ is the positive constant, ρ_{CNT} stands for density, k_{CNT} is thermal conductivity and the heat capacity $(\rho C_p)_{CNT}$.

Moreover, S the non-dimensional parameter and suction is ($S > 0$) or injection ($S < 0$).
ϕ is the volume fraction of CNT nanoparticles in Table 1. ρ_f stands for the density of sodium alginate, and k_f represents its thermal conductivity. This study examined the thermal characteristics of CNTs using the Yamada–Ota thermal conductivity model (Table 2).

Table 2: Thermophysical properties of suspended nanofluid made of CNTs (see [23,24])

Density	$\rho_{cnt} = (1-\phi)\rho_f + \phi\rho_s$
Viscosity	$\mu_{nf}(T) = \frac{\mu_f(T)}{(1-\phi)^{2.5}}$
Heat capacity	$(\rho C_p)_{cnt} = (1-\phi)(\rho C_p)_f + \phi(\rho C_p)_s$
Thermal conductivity (Yamada–Ota model)	$\frac{k_{nf}}{k_f} = \frac{1+\frac{k_f}{k_s}\frac{L}{R}\phi^{0.2} + \left(1-\frac{k_f}{k_s}\right)\phi\frac{L}{R}\phi^{0.2} + 2\phi\left(\frac{k_s}{k_s-k_f}\right)\ln\left(\frac{k_s+k_f}{2k_s}\right)}{1-\phi+2\phi\left(\frac{k_f}{k_s-k_f}\right)\ln\left(\frac{k_s+k_f}{2k_s}\right)}$

A stream function ψ was devised to resolve the boundary-layer equations (see refs. [50,51]), where $u = \frac{\partial\psi}{\partial y}$ and $v = -\frac{\partial\psi}{\partial x}$, in order to find a solution that is comparable to the one in Eqs. (1), (2), and (5), which led to the exact satisfaction of (1). We are able to obtain the variations in similarity (see refs. [50,51]):

$$\psi = (2u_e\nu_f)^{\frac{1}{2}} f(\eta), \quad T = T_\infty[1 + (\theta_w - 1)\theta(\eta)],$$
$$\theta_w = \frac{T_w}{T_\infty}, \quad \eta = y\left(\frac{u_e}{2\nu_f x}\right)^{\frac{1}{2}}. \tag{7}$$

The modified versions of the momentum and energy equations are obtained as follows by inserting Eq. (7) into Eqs. (2) and (5):

$$\frac{1}{(1-\phi)^{2.5}}\left(1 + \frac{1}{\beta}\right)[(1 + \Omega - \Omega\theta)f''' - \Omega\theta' f''] + ff'' - f'^2 + 1 = 0, \tag{8}$$

$$\left(\left(\frac{k_{CNT}}{k_f} + \mathrm{Rd}(1 + (\theta_w - 1)\theta)^3\right)\theta'\right)' + \mathrm{Pr}_f(T)\frac{(\rho C_p)_{CNT}}{(\rho C_p)_f} f\theta' = 0. \tag{9}$$

Transformation of BCs (6) into

$$f(0) = S, f'(0) = \lambda, \quad \theta(0) = 1,$$
$$f'(\eta) \to 1, \theta(\eta) \to 0, \text{as } \eta \to \infty. \tag{10}$$

2.1 Variable Prandtl number

As Prandtl number depends on viscosity, so for variable viscosity, the variable Prandtl number is defined as a result of the variations in viscosity throughout the boundary layer. $\mathrm{Pr}_f(T) = \frac{\mu_{nf}(T)C_p}{k_f} = \frac{\left(\frac{\Omega-\theta}{\Omega}\right)\mu_{nf}(T)C_p}{k_f}$, so, we obtain $\mathrm{Pr}_f = \mathrm{Pr}_f(T)\left(1 - \frac{\theta}{\Omega}\right)\frac{k_f}{\mu_{nf}(T)C_p}$. So applying this in Eq. (10), we obtain

$$\left(\left(\frac{k_{CNT}}{k_f} + \mathrm{Rd}(1 + (\theta_w - 1)\theta)^3\right)\theta'\right)' + \mathrm{Pr}_f(T)\left(1 - \frac{\theta}{\Omega}\right)\frac{k_f}{\mu_{nf}(T)C_p}\frac{(\rho C_p)_{CNT}}{(\rho C_p)_f} f\theta' = 0, \tag{11}$$

where β is the Casson parameter, S is the mass suction, λ is the shrinking parameter, Rd is the radiation, and θ_w is the temperature ratio parameter.

The local Nusselt number (represented as Nu_x,) and the skin friction coefficient (represented as C_{fx}) are the two physical parameters that are the subject of the investigation. Here is how these quantities are defined:

$$C_{\mathrm{fx}} = \frac{\tau_{\tilde{w}x}}{\rho_f U^2}, \mathrm{N\tilde{u}}_x = \frac{xq_{\tilde{w}}}{k_{\mathrm{f}}(T_{\mathrm{w}} - T_\infty)}, \tag{12}$$

where $\tau_{\tilde{w}x}$ represents the x-axis shear stress and $q_{\tilde{w}}$ represents the heat flux. The following terms may be defined as

$$\begin{aligned} \tau_{\tilde{w}x} &= \mu_{\mathrm{nf}}(T)\left(1 + \frac{1}{\beta}\right)\left(\frac{\partial u}{\partial y}\right)_{z=0}, \\ q_{\tilde{w}} &= -k_{\mathrm{CNT}}\left[\left(\frac{\partial T}{\partial z}\right)_{z=0} + (q_{\mathrm{r}})_{y=0}\right]. \end{aligned} \tag{13}$$

By solving Eqs. (7), (12), and (13), we obtain the following results:

$$\begin{aligned} \mathrm{Re}_x^{1/2} C_{\mathrm{fx}} &= \frac{\mu_{\mathrm{nf}}}{\left(\frac{\Omega - \theta}{\Omega}\right)}\left(1 + \frac{1}{\beta}\right) f''(0), \\ \mathrm{Re}_x^{-1/2}\mathrm{Nu}_x &= -\left(\frac{k_{\mathrm{CNT}}}{k_{\mathrm{f}}} + \mathrm{Rd}(1 + (\theta_{\mathrm{w}} - 1)\theta(0))^3\right)\theta'(0), \end{aligned} \tag{14}$$

where $\mathrm{Re}_x = \frac{u_e x}{\upsilon_{\mathrm{f}}}$ denote the local Reynolds number.

3 Solution methodology with code validation

It is very important to use the RK-IV method along with similarity transformations to solve differential equations for many good reasons: when you use RK-IV along with similarity transformations, you can solve differential equations. This lets you see the basic physical rules that control the system. It is possible for researchers to obtain substantial insights into the behavior of a system by gaining knowledge of how the solution undergoes evolution across time or space. The Runge–Kutta–Fehlberg (RKF) method is used for computer solving of linked nonlinear differential equations. Equations (8) and (11), as well as boundary conditions (10), are solved using RKF with shooting technique. The system is divided using a shooting approach into a series of initial value problem, which are then solved by applying the RKF method. A numerical solution with a maximum value of $\eta_{\max} = 15$ is obtained using a step size of $\Delta\eta = 0.001$, to guarantee convergence and accuracy up to the fifth decimal place.

$$m_1 = f, \quad m_2 = f', \quad m_3 = f'', \quad n_1 = \theta, \quad n_2 = \theta'. \tag{15}$$

By Eq. (14),

$$m_1' = f', \quad m_3' = m_4 = f''', \quad n_1' = \theta', n_2' = \theta'' = n_3. \tag{16}$$

The conclusions drawn from Eqs. (15) and (16) are as follows:

$$m_1' = m_2, m_2' = m_3, m_4 = f''', n_2' = n_3 = \theta''. \tag{17}$$

Eq. (17) gives the values of f''' and θ'' as follows:

$$\begin{aligned} m_4 = -(1 - \phi)^{2.5} &\frac{1}{(1 + \Omega - \Omega n_1)\left(1 + \frac{1}{\beta}\right)} \\ &\times [-\Omega n_2 m_3 - m_1^2 + 1], \end{aligned} \tag{18}$$

$$\begin{aligned} n_3 = \mathrm{Pr}_{\mathrm{f}}(T)&\left(1 - \frac{n_1}{\Omega}\right)\frac{k_{\mathrm{f}}}{\mu_{\mathrm{nf}}(T)C_{\mathrm{p}}} \\ &\times \frac{\frac{(\rho C_{\mathrm{p}})_{\mathrm{CNT}}}{(\rho C_{\mathrm{p}})_{\mathrm{f}}}}{\left(\frac{k_{\mathrm{CNT}}}{k_{\mathrm{f}}} + \mathrm{Rd}(1 + (\theta_{\mathrm{w}} - 1)\theta)^3\right)}[m_1 n_2], \end{aligned} \tag{19}$$

$$m_1 = S, \qquad m_2 = \lambda, \qquad n = 1, \quad m_2 \to 1, \quad n \to 0. \tag{20}$$

A computational software program called Mathematica is used to perform the numerical simulations and graphical analyses.

The findings reported in Table 3 align well with the solution obtained by Tadesse *et al.* [53] for a typical fluid example. We assure you that the approach used to address our issue is precise and reliable.

4 Results and discussion

This study investigates the steady two-dimensional axisymmetric boundary layer of a Casson nanofluid containing CNTs with single and multiple walls. The nanofluid flows in a uniformly free stream across a permeable plate. Applying suitable similarity transformations converts the

Table 3: Calculating $\mathrm{Re}_x^{1/2} C_{\mathrm{fx}}$ and $\mathrm{Re}_x^{-1/2}\mathrm{Nu}_x$ for various values of the shrinking parameter, using $\mathrm{Pr} = 1$ for $\phi = \mathrm{Rd} = \theta_{\mathrm{w}} = S = \Omega = 0 = 0$ (regular fluid)

	$\mathrm{Re}_x^{1/2} C_{\mathrm{fx}}$		$\mathrm{Re}_x^{-1/2}\mathrm{Nu}_x$	
λ	**Present**	**Tadesse *et al.* [53]**	**Present**	**Tadesse *et al.* [53]**
−0.25	1.40224	1.402241	0.66857	0.668573
−0.5	1.49567	1.495670	0.50145	0.501448
−0.75	1.48930	1.489298	0.29378	0.293763
−1.0	1.32882	1.328817	0	0

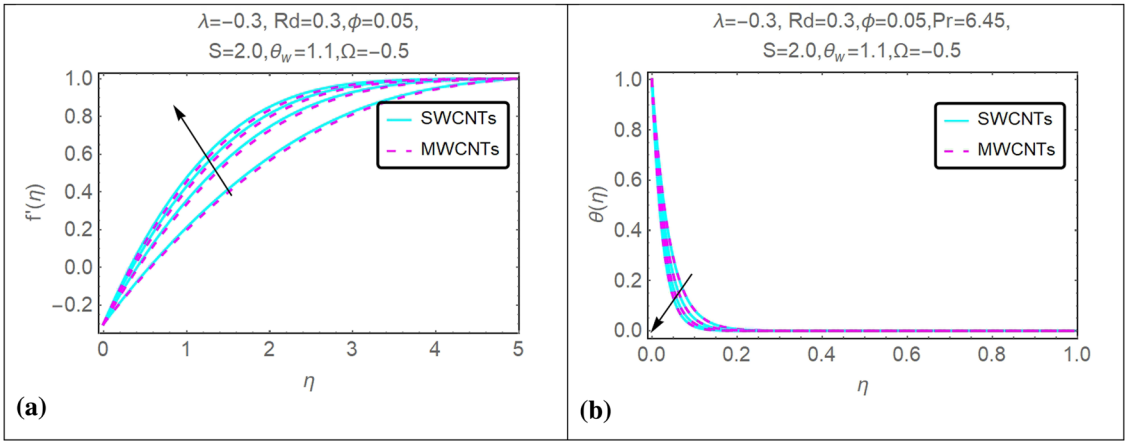

Figure 2: (a) and (b) Influence of β = 0.5, 1.0, 1.5, 2.0 on $f'(\eta)$ and $\theta(\eta)$ profile.

controlling system of partial differential equations into a collection of ordinary differential equations (ODEs). This system of ODEs is then solved analytically to obtain velocity and temperature distributions. The influence of SWCNTs and MWCNTs is examined graphically for various parameters, including volume fraction ϕ, mass suction S, stretching parameter λ, Casson parameter β, temperature ratio parameter θ_w, and thermal radiation parameter Rd.

The range of parameters are as follows: $-1.0 \le \lambda \le 0.0$ (shrinking), $0.0 \le \text{Rd} \le 1.0$ (radiation), $1.0 \le \theta_w \le 2.0$ (temperature ratio), $1.0 \le S \le 2.5$ (mass suction), $0.5 \le \beta \le 3.0$ (Casson), $-0.5 \le \Omega \le -3.0$ (variable viscosity), and $2.0 \le \text{Pr} \le 10.0$ (Prandtl number). The range of these parameters has been selected in a manner that ensures the satisfaction of boundary conditions.

Figure 2(a) and (b) presents the impact of β on velocity $f'(\eta)$ and temperature $\theta(\eta)$ profiles of CNTs, specifically SWCNTs and MWCNTs. Upon examining Figure 2(a) and (b), it is evident that the velocity profile shows a positive correlation with greater values of β, but the temperature profile has a negative correlation. The graph illustrates that as the values of β increase, the fluid velocity $f'(\eta)$ increases and the temperature $\theta(\eta)$ decreases. This can be attributed to the stronger viscous force experienced by the flow, resulting in a reduction of the momentum layer and an expansion of the thermal layer. MWCNTs shows better results in this case for velocity profile.

Figure 3(a) and (b) illustrates the stimulus of the Prandtl parameter (Pr) on the velocity $f'(\eta)$ and temperature $\theta(\eta)$ profiles, respectively. It is noted that with expanding values of Prandtl parameter, the velocity profile of CNTs (SWCNTs and MWCNTs) increases, whereas temperature profile decreases. When it comes to the moving plate, a greater Pr indicates that momentum diffusivity is more relevant than thermal diffusivity. Because of this imbalance, the transmission of momentum is more effective than the transfer of heat from one fluid medium

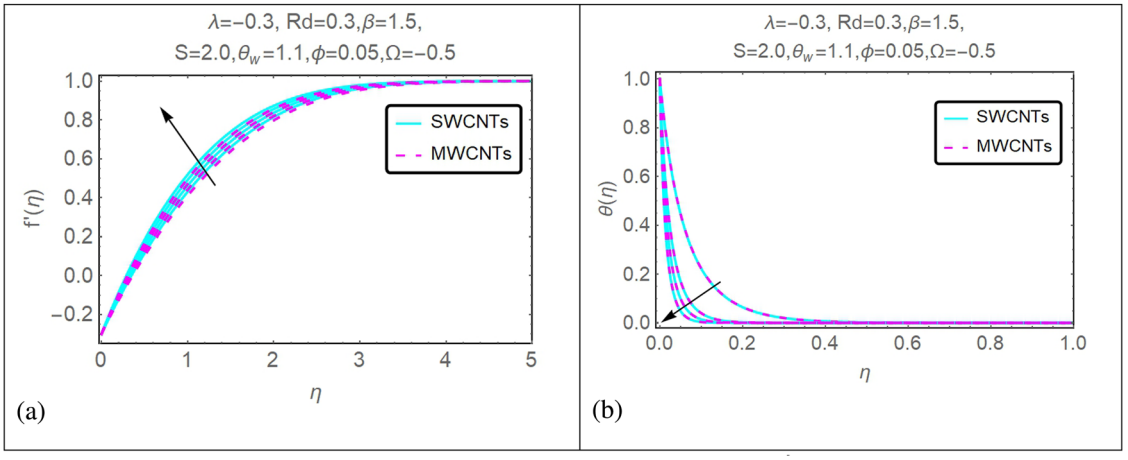

Figure 3: (a) and (b) Impact of Pr = 3.0, 6.45, 8.0, 10.0 on $f'(\eta)$ and $\theta(\eta)$.

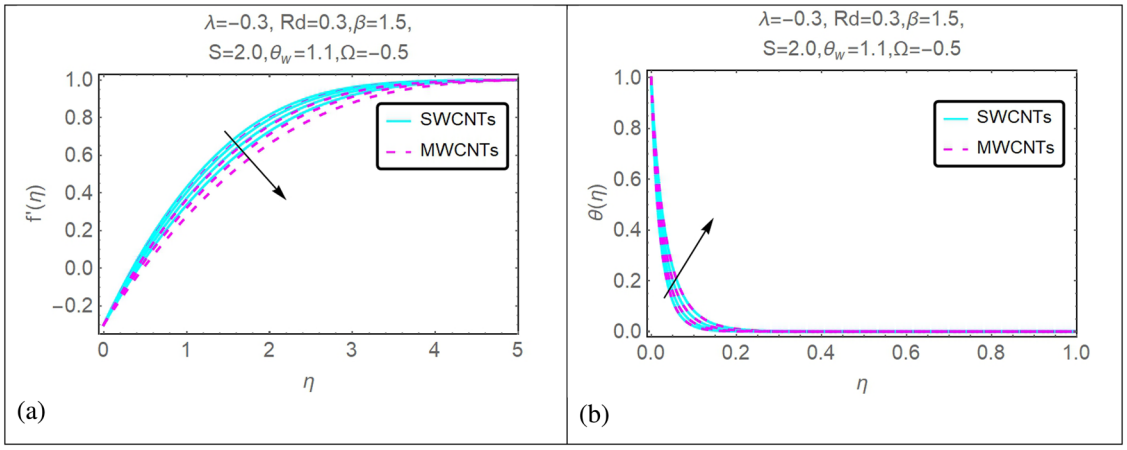

Figure 4: (a) and (b) Influence of ϕ = 0.01, 0.03, 0.05, 0.07 on $f'(\eta)$ and $\theta(\eta)$.

to another. In this way, the fluid can more readily surpass its yield stress, resulting in an improvement in flow behavior and velocity profile. An increase in the Pr suggests that momentum diffusivity is more important than thermal diffusivity. Because of this discrepancy, temperature gradients diffuse less effectively than momentum gradients, resulting in a lower temperature profile.

Figure 4(a) and (b) demonstrates the consequence of the volume fraction ϕ on the velocity $f'(\eta)$ and temperature $\theta(\eta)$ profiles of CNT's suspended nanofluid. Notably, the viscosity of the liquid is enhanced as the volume percentages of nanoparticles rise. Figure 4(a) shows that the fluid velocity decreases due to higher viscous forces. Additionally, Figure 4(a) shows that velocity distributions decrease as the ϕ of CNT's nanoparticles increase, which is due to the thickening of the momentum boundary layer. The increase in volume fractions of CNT's nanoparticles results in a denser behavior of the suspended nanofluid, leading to an augmented thermal boundary-layer thickness. Consequently, higher volume fractions enhance the thermal characteristics of the CNT's suspended nanofluid, as indicated in Figure 4(b). The temperature of the fluid is directly related to the width of the thermal boundary layer. By introducing appropriate nanoparticles, there is a notable elevation in temperature of base fluid due to the high thermal conductivity and low temperature gradient exhibited by CNTs in comparison with the base fluid. Notably, the temperature of multi-walled nanoparticles is lower than that of single-walled nanoparticles, which can be attributed to the lower density of MWCNTs.

Figure 5(a) displays the distribution of the $f'(\eta)$ with veneration to the suction parameter (S). The results indicate that an upsurge in S consequences in a corresponding upsurge in $f'(\eta)$ within the velocity profile of the solution. Furthermore, there exists a direct relationship between the increase in S and the flow resistance measured by $f'(\eta)$. In Figure 5(b), temperature profile of CNTs is shown for

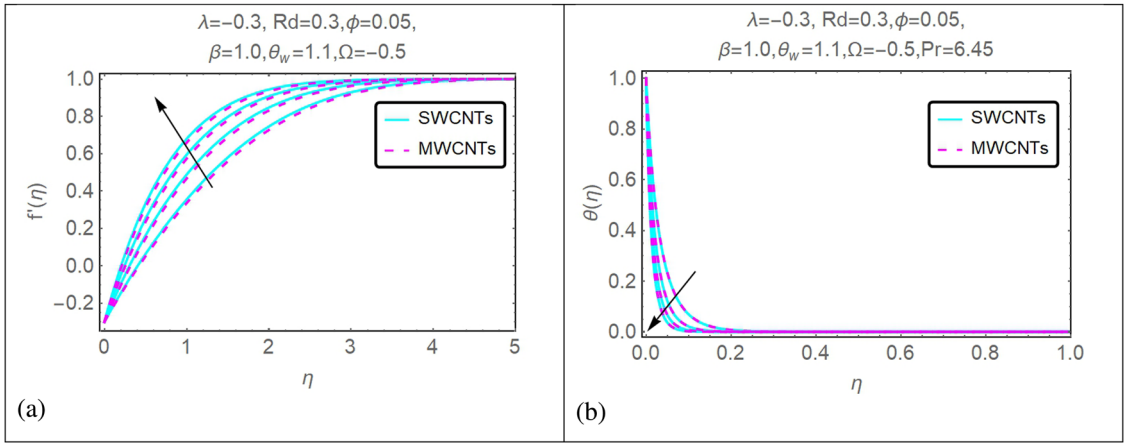

Figure 5: (a) and (b) Impact of S = 1.0, 1.5, 2.0, 2.5 on $f'(\eta)$ and $\theta(\eta)$.

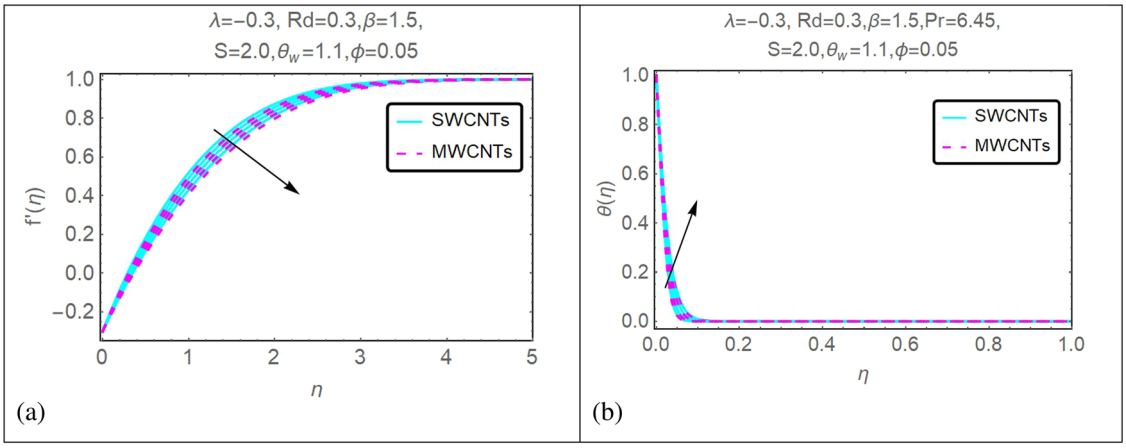

Figure 6: (a) and (b) Impact of Ω = –0.5, 0, –1.0, –1.5, –2.0 on $f'(\eta)$ and $\theta(\eta)$.

different suction values. The graph illustrates a decreasing pattern in temperature profile as suction parameter increases. Because of the increase in the suction parameter, the fluid travels more quickly and exceeds the threshold for its yield stress. The rising velocity profile demonstrates that there is more flow because of this event has increased flow. An upsurge in the S parameter leads to a reduction in the temperature $\theta(\eta)$ profile. The temperature profile decreases as more fluid is evacuated from the plate region. As a result, the shortened residence time for heat exchange between the fluid and the plate causes a drop in the temperature gradient, which subsequently alters the $\theta(\eta)$ profile.

Figure 6(a) and (b) examines the impact of the parameter Ω on velocity and temperature $\theta(\eta)$ distribution. The graph demonstrates that velocity profile is decreasing, while temperature for both CNTs is showing an increasing behavior. Adding CNTs to the nanofluid may have additional effects on the velocity profile owing to the distinctive characteristics of CNTs. In this scenario, however, the primary effect of the viscosity parameter may be greater than that of other components, resulting in a decreased velocity profile. Changing the viscosity parameter usually leads to a rise in the $\theta(\eta)$ profile. Increased viscosity leads to increased fluid resistance, causing a rise in internal friction within the unit. Increasing the level of friction inside the system dissipates more energy as heat, leading to a rise in the $\theta(\eta)$ profile.

Figure 7(a) and (b) examines the impact of the parameters Rd and θ_w on temperature distribution. The graph proves that advanced values of Rd and θ_w lead to an increase in temperature for both CNTs. As the Rd parameter upsurges, the heat transfer process inside the fluid becomes more intense, resulting in a greater exchange of thermal energy between the fluid and the environment in which it is located. This leads to a rise in the temperature profile, and because of the situation, the temperature profile rises. A higher temperature ratio indicates a larger temperature difference between the fluid and its surroundings. The heightened temperature

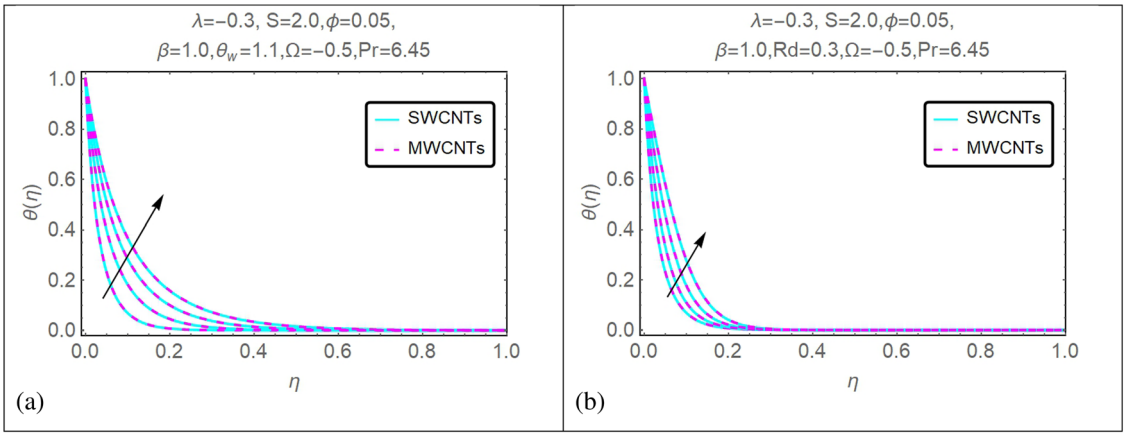

Figure 7: (a, b) Impact of Rd = 0.1, 0.3, 0.5, 0.7 and θ_w = 1.1, 1.2, 1.3, 1.4 on $\theta(\eta)$.

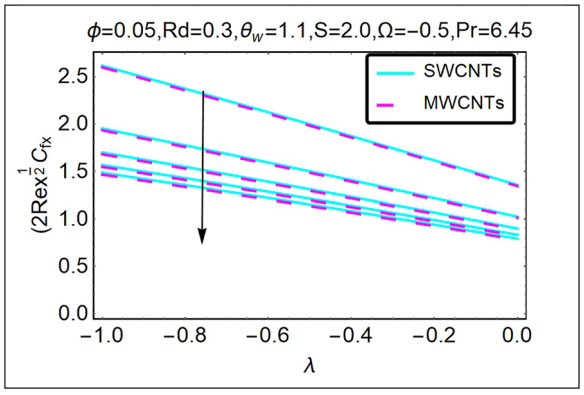

Figure 8: Impact of β = 0.5, 1.0, 1.5, 2.0, 2.5 with λ on $\mathrm{Re}_x^{1/2}C_{\mathrm{fx}}$.

gradient speeds up thermal energy transmission, enabling the fluid to absorb more heat from its surroundings. The fluid's temperature gradient increases.

Figure 8 depicts the influence of Casson parameter β and shrinking parameter λ on skin friction $\mathrm{Re}_x^{1/2}C_{\mathrm{fx}}$. The findings reveal that $\mathrm{Re}_x^{1/2}C_{\mathrm{fx}}$ decreases as value of β and λ upsurges. A component known as yield stress is incorporated into the Casson model. This word indicates the minimal stress that is required to commence flow. There is a direct correlation between an increased Casson parameter and an increase in yield stress. This increased yield stress indicates that a bigger force is required for the commencement of flow, which ultimately results in a lesser amount of skin friction. It is possible to establish a connection between the shrinked parameter in nanofluids and the alignment or orientation of nanoparticles within the fluid. The alignment of nanoparticles can result in an increase in viscosity and a reduction in flow of fluid. With an increase in shrinked parameter, this alignment effect becomes more pronounced, which contributes to a decrease in amount of skin friction.

Figure 9(a) and (b) presents the impact of suction parameter S on skin friction $\mathrm{Re}_x^{1/2}C_{\mathrm{fx}}$, and Nusselt number $\mathrm{Re}_x^{-1/2}\mathrm{Nu}_x$ with the values indicating an apparent increase in $\mathrm{Re}_x^{1/2}C_{\mathrm{fx}}$ and $\mathrm{Re}_x^{-1/2}\mathrm{Nu}_x$ compared to its actual value. It is important to note this discrepancy. The inclusion of the suction component decelerates the motion of CNTs, leading to an increased velocity difference alongside of permeable moving plate. This introduces an unexpected velocity gradient due to the suction effect. Consequently, near-wall fluid motions responsible for heat transfer are initiated, and the buoyant forces induced by influence of strong viscosity are attenuated. Suction induces the formation of an unforeseen velocity gradient.

Figure 10(a) and (b) presents the impact of variable viscosity parameter Ω with λ on skin friction $\mathrm{Re}_x^{1/2}C_{\mathrm{fx}}$, and Nusselt number $\mathrm{Re}_x^{-1/2}\mathrm{Nu}_x$ with the values indicating an apparent increase in skin friction and a decrease in Nusselt number compared to its actual value. Changing the viscosity parameter of the Casson nanofluid increases its resistance to flow, resulting in heightened frictional forces acting on the fluid along the surface of the moving plate. This disorder causes the skin to become more susceptible to friction. The Nusselt number tells us about the convective heat transfer rate and how thick the thermal barrier layer is. As its viscosity and factors decrease, the fluid's flow resistance increases. This makes the temperature boundary layer thicker. Because this thicker border layer makes it harder for heat to move through convection, the Nusselt number goes down.

Figure 11(a) and (b) presents the impact of parameter ϕ with λ on skin friction $\mathrm{Re}_x^{1/2}C_{\mathrm{fx}}$, and Nusselt number $\mathrm{Re}_x^{-1/2}\mathrm{Nu}_x$ with the values indicating an apparent increase in $\mathrm{Re}_x^{1/2}C_{\mathrm{fx}}$ and $\mathrm{Re}_x^{-1/2}\mathrm{Nu}_x$ compared to its actual value. A larger volume fraction number implies a greater concentration of

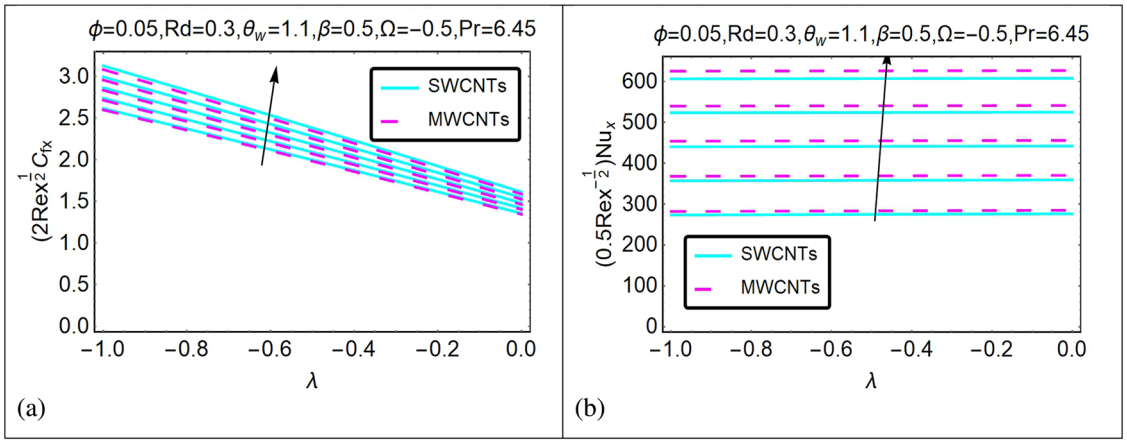

Figure 9: (a) and (b) Impact of S = 1.0, 1.5, 2.0, 2.5 with λ on $\mathrm{Re}_x^{1/2}C_{fx}$ and $\mathrm{Re}_x^{-1/2}\mathrm{Nu}_x$.

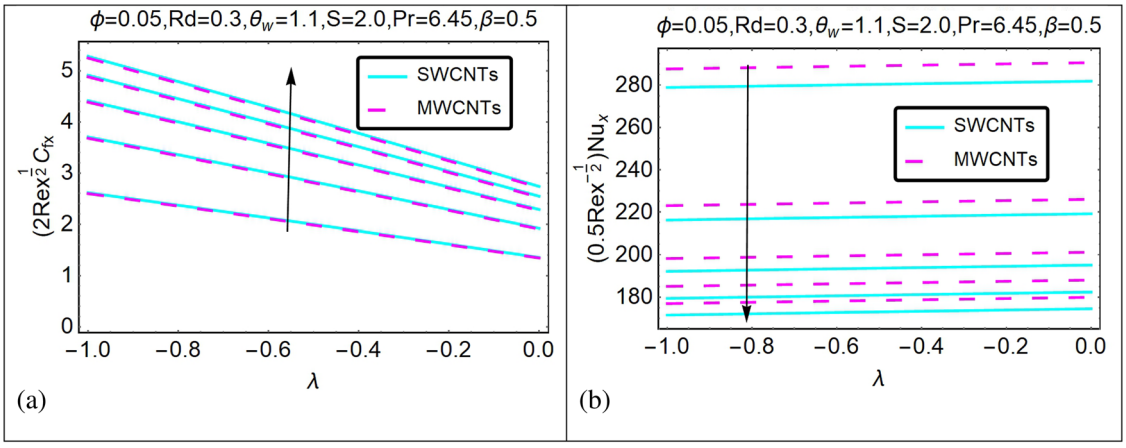

Figure 10: (a) and (b) Impact of Ω = −0.5, −1.0, −1.5, −2.0, −2.5 with λ on $\mathrm{Re}_x^{1/2}C_{fx}$ and $\mathrm{Re}_x^{-1/2}\mathrm{Nu}_x$.

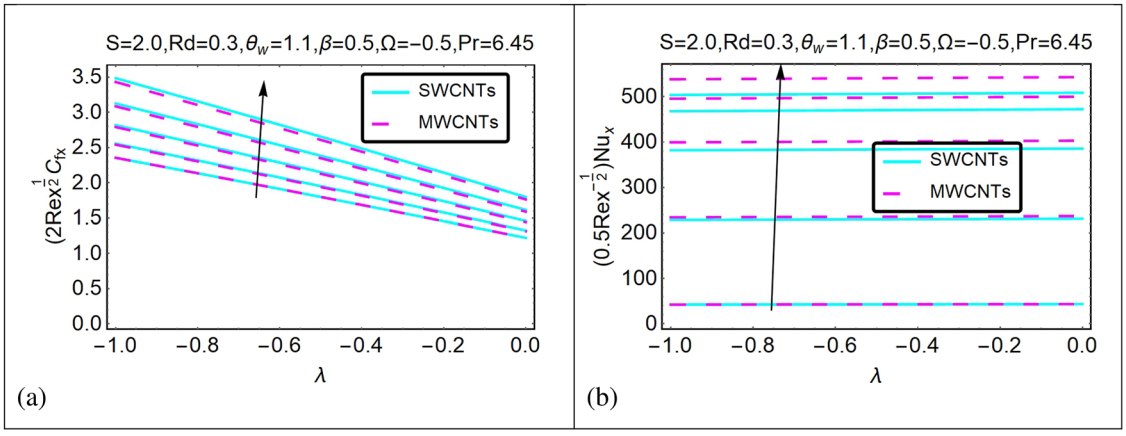

Figure 11: (a) and (b) Impact of ϕ = 0.02, 0.04, 0.06, 0.08, 0.1 with λ on $\mathrm{Re}_x^{1/2}C_{fx}$ and $\mathrm{Re}_x^{-1/2}\mathrm{Nu}_x$.

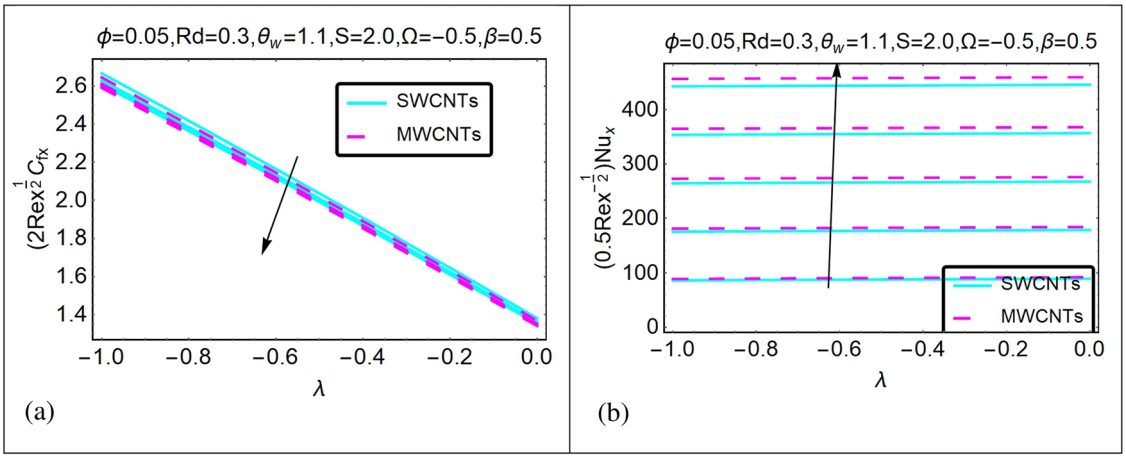

Figure 12: (a) and (b) Impact of Pr = 2.0, 4.0, 6.0, 8.0, 10.0 with λ on $\mathrm{Re}_x^{1/2}C_{fx}$ and $\mathrm{Re}_x^{-1/2}\mathrm{Nu}_x$.

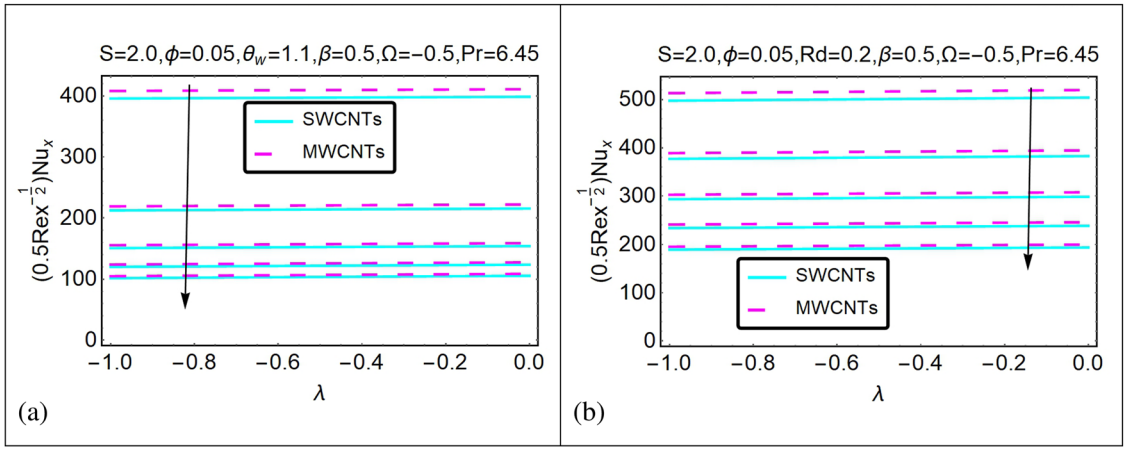

Figure 13: (a) and (b) Impact of Rd = 0.1, 0.3, 0.5, 0.7, 0.9 with λ and θ_w = 1.1, 1.2, 1.3, 1.4, 1.5 with λ on $\mathrm{Re}_x^{-1/2}\mathrm{Nu}_x$.

nanoparticles in the nanofluid, leading to an increased number of nanoparticles in the nanofluid. Increasing the fluid's viscosity results in an increase in the frictional forces that the fluid encounters along the surface of the moving plate. As a result, skin friction increases. Nanoparticles have a noteworthy surface area-to-volume ratio in comparison with other particles. At the same time, as there is an increase in volume percentage of nanoparticles, there is a corresponding increase in the surface area that is available for heat exchange. Because of this augmented surface area, the fluid can transport heat more efficiently to its surroundings, which eventually leads to an upsurge in $\mathrm{Re}_x^{-1/2}\mathrm{Nu}_x$.

Figure 12(a) and (b) examines the impact of the Prandtl parameter Pr with λ on skin friction and Nusselt number. Skin friction is decreasing, while Nusselt number is increasing, as shown in Figure 12(a) and (b). Increases in the Prandtl value are associated with an increase in thermal diffusivity in comparison with momentum diffusivity. As a result, the fluid is more effective at transmitting heat than it is at transferring momentum, which helps to reduce viscous effects and skin friction. Increasing the Prandtl parameter significantly raises the thermal diffusivity of the fluid compared to its viscosity. Reducing the thickness of the thermal boundary layer improves convective heat transfer. The Nusselt number increases.

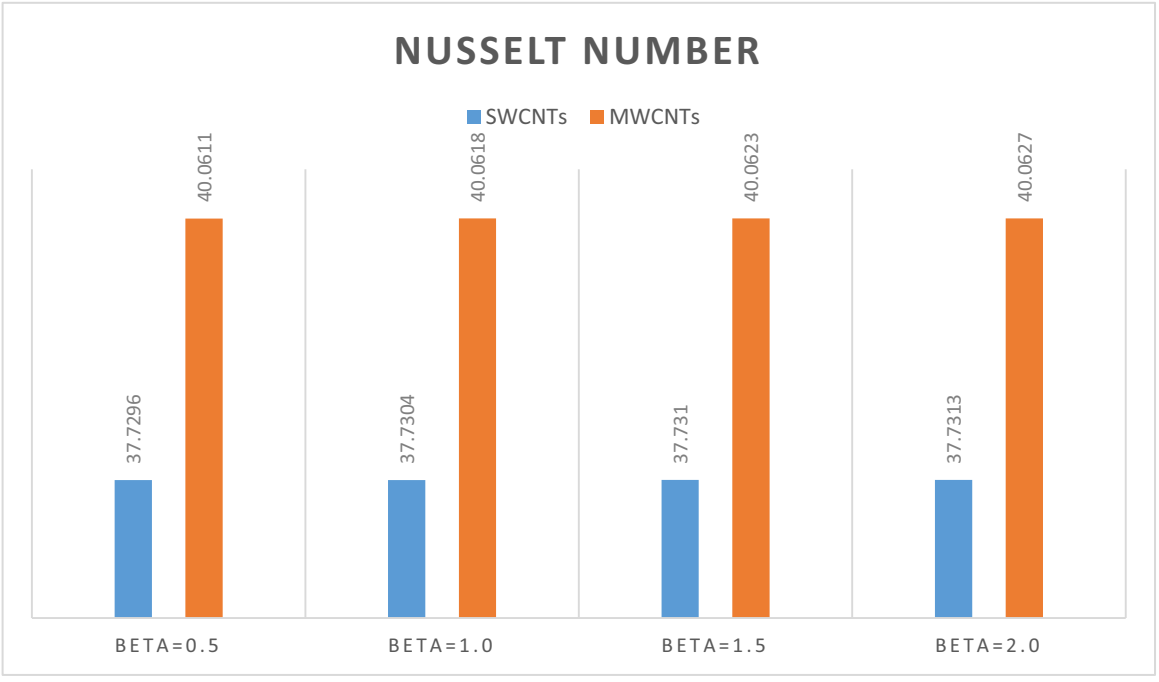

Figure 14: Impact of β = 0.5, 1.0, 1.5, 2.0 on $\mathrm{Re}_x^{-1/2}\mathrm{Nu}_x$.

Figure 13(a) and (b) shows the effect of radiation parameter Rd and θ_w with λ on $\mathrm{Re}_x^{-1/2}\mathrm{Nu}_x$. Heat transfer rate is decreasing for both variations. With an upsurge in the radiation parameter, it has been observed that the impact of radiation heat transfer becomes more pronounced. The efficiency of thermal radiation in enabling heat transfer through convection is often lower when compared to the efficiency of other mechanisms such as conduction and convection. There is a possibility that the presence of radiation will reduce the overall convective heat transfer, which will ultimately lead to a reduction in the Nusselt number. The occurrence of this scenario will take place if radiation has a noteworthy impact on the process of heat transfer. An increased temperature ratio and a stretched parameter may alter fluid flow dynamics and thermal properties. An increased temperature ratio may enhance convective heat transfer, while a stretched parameter can affect fluid flow patterns and thermal boundary-layer thickness. These factors influence the Nusselt number through their varying amplitude and direction.

Figure 14 shows the influence of β on $\mathrm{Re}_x^{-1/2}\mathrm{Nu}_x$ for both SWCNTs and MWCNTs. Heat transfer rate is increasing with an increase in Casson parameter, and it shows that result for MWCNTs is much better than SWCNTs. A yield stress term is included in the Casson model, which represents the lowest stress required to initiate fluid flow. The yield stress increases in tandem with an increase in the Casson parameter. The increased yield stress promotes a more steady and regulated flow, which enhances the properties of heat transfer. One factor that improves heat transfer is the fluid's capacity to flow effectively even when there is a yield stress.

5 Conclusion

The main aim of this research is to examine the impact of ϕ, β, λ, S, Rd, Pr, Ω, and θ_w on velocity, temperature, skin friction, and heat transfer. The methodology and results have been thoroughly discussed, yielding several key findings. RK-IV with shooting method is used to solve the differential equations. The key findings of the current study are as follows:

- Higher values of Casson parameter β enhance the fluid velocity while decelerating the temperature field.
- The velocity of CNT's suspended nanofluid (both SWCNTs and MWCNTs) decreases with increasing shrinking parameter λ, while temperature profiles increase.
- Additionally, an increase in solid volume fraction ϕ leads to higher temperatures.
- Moreover, larger mass suction S enhances velocity and reduces temperature.
- The findings reveal that the skin friction coefficient $\mathrm{Re}_x^{1/2}C_{fx}$ rises as the values of β and λ increase along with ϕ.
- The results indicate that the Nusselt number $\mathrm{Re}_x^{-1/2}\mathrm{Nu}_x$ increases with higher values of ϕ, β, λ, and S.
- The skin friction $\mathrm{Re}_x^{1/2}C_{fx}$ reduces, while the Nusselt number $\mathrm{Re}_x^{-1/2}\mathrm{Nu}_x$ upsurges with an increase in Prandtl number.
- The rate of heat transfer and the quantity of skin friction are both affected by changes in the viscosity parameter.
- The Nusselt number decreases with increasing values of Rd and θ_w.

To handle the nonlinear equations that dictate the behavior of Casson fluids that contain CNTs above a permeable moving plate, it is possible to develop advanced numerical approaches or computational tools. It is possible that this endeavor will involve the application of finite element methods, finite volume methods, or other alternative methodologies within the field of CFD. Investigate the ways in which the dynamics of fluids, heat transport, and rheological behavior are affected by the features that are inherent to CNTs, such as their length and radius. Investigate the potential implications that different types of nanoparticles or hybrid nanomaterials could have on the system. This study should investigate more than just simple models of thermal radiation. It should also include variables that change based on temperature and how radiative heat transfer affects the overall properties of fluid flow and heat transfer.

Acknowledgments: Researchers Supporting Project Number (RSPD2024R1060), King Saud University, Riyadh, Saudi Arabia.

Funding information: The study was funded by Researchers Supporting Project Number (RSPD2024R1060), King Saud University, Riyadh, Saudi Arabia.

Author contributions: K. R., Z.M., and A: conceptualization, methodology, software, formal analysis, validation, and writing – original draft. U.K.: writing – original draft, data curation, investigation, visualization, supervision, and validation. B.A.: conceptualization, writing – original draft, writing – review and editing, and resources. F.A.A. and E.A.A.I: validation, investigation, writing – review and editing, formal analysis, project administration, funding acquisition, and software. All authors have accepted responsibility for the entire content of this manuscript and approved its submission.

Conflict of interest: The authors state no conflict of interest.

References

[1] Hamid M, Usman M, Khan ZH, Ahmad R, Wang W. Dual solutions and stability analysis of flow and heat transfer of Casson fluid over a stretching sheet. Phys Lett A. 2019 Jul;383(20):2400–8.

[2] Jamshed W, Uma Devi SS, Goodarzi M, Prakash M, Sooppy Nisar K, Zakarya M, et al. Evaluating the unsteady Casson nanofluid over a stretching sheet with solar thermal radiation: An optimal case study. Case Stud Therm Eng. 2021 Aug;26:101160.

[3] Gomathi N, De P. Impact of hall currents and ion slip on mixed convective casson williamson nanofluid flow with viscous dissipation through porous medium. Nanosci Technol Int J. 2024;15.

[4] Poulomi D, Ekambaram S. Bioconvective Casson nanofluid flow toward stagnation point in non-Darcy porous medium with buoyancy effects, chemical reaction, and thermal radiation. Heat Transfer. Wiley Online Library [Internet]; 2023. [cited 2024 Feb 22]. https://onlinelibrary.wiley.com/doi/full/10.1002/htj.22753.

[5] Vinodkumar Reddy M, Vajravelu K, Lakshminarayana P, Sucharitha G. Heat source and Joule heating effects on convective MHD stagnation point flow of Casson nanofluid through a porous medium with chemical reaction. Numer Heat Transf Part B Fundam. 2024 Mar;85(3):286–304.

[6] Awan AU, Ahammad NA, Shatanawi W, Allahyani SA, Tag-ElDin EM, Abbas N, et al. Significance of magnetic field and Darcy–Forchheimer law on dynamics of Casson-Sutterby nanofluid subject to a stretching circular cylinder. Int Commun Heat Mass Transf. 2022 Dec;139:106399.

[7] Abbas N, Shatanawi W, Abodayeh K. Computational analysis of MHD nonlinear radiation casson hybrid nanofluid flow at vertical stretching sheet. Symmetry. 2022 Jul;14(7):1494.

[8] Lanjwani HB, Saleem S, Chandio MS, Anwar MI, Abbas N. Stability analysis of triple solutions of Casson nanofluid past on a vertical exponentially stretching/shrinking sheet. Adv Mech Eng. 2021 Nov;13(11):16878140211059679.

[9] Reddy MV, Lakshminarayana P. Cross-diffusion and heat source effects on a three-dimensional MHD flow of Maxwell nanofluid over a stretching surface with chemical reaction. Eur Phys J Spec Top. 2021 Jul;230(5):1371–9.

[10] Maleki H, Safaei MR, Alrashed AAAA, Kasaeian A. Flow and heat transfer in non-Newtonian nanofluids over porous surfaces. J Therm Anal Calorim. 2019 Feb;135(3):1655–66.

[11] Amjad M, Zehra I, Nadeem S, Abbas N, Saleem A, Issakhov A. Influence of Lorentz force and induced magnetic field effects on casson micropolar nanofluid flow over a permeable curved stretching/shrinking surface under the stagnation region. Surf Interfaces. 2020 Dec;21:100766.

[12] Kasim ARM, Arifin NS, Ariffin NAN, Salleh MZ, Anwar MI. Mathematical model of simultaneous flow between casson fluid and dust particle over a vertical stretching sheet. Int J Integr Eng. 2020 Feb;12(3):253–60.

[13] Adnan, Ashraf W. Thermal efficiency in hybrid (Al_2O_3-CuO/H_2O) and ternary hybrid nanofluids (Al_2O_3-CuO-Cu/H_2O) by considering the novel effects of imposed magnetic field and convective heat condition. Waves Random Complex Media. 2022 Jul;1–16.

[14] Ahmed N, Adnan, Khan U, Mohyud-Din ST. Influence of thermal radiation and viscous dissipation on squeezed flow of water between Riga plates saturated with carbon nanotubes. Colloids Surf Physicochem Eng Asp. 2017 Jun;522:389–98.

[15] Maleki H, Safaei MR, Togun H, Dahari M. Heat transfer and fluid flow of pseudo-plastic nanofluid over a moving permeable plate with viscous dissipation and heat absorption/generation. J Therm Anal Calorim. 2019 Feb;135(3):1643–54.

[16] Alazwari MA, Abu-Hamdeh NH, Goodarzi M. Entropy optimization of first-grade viscoelastic nanofluid flow over a stretching sheet by using classical Keller-box scheme. Mathematics. 2021 Jan;9(20):2563.

[17] Mahmood Z, Khan U. Mixed convective flow of nanofluid across exponential surface: A numerical assessment of the impact of Darcy-Forchheimer and nanoparticle aggregation. Numer Heat Transf Part Appl. 2023 Nov;1–26.

[18] Xue QZ. Model for thermal conductivity of carbon nanotube-based composites. Phys B Condens Matter. 2005 Nov;368(1):302–7.

[19] Shahzad F, Jamshed W, Eid MR, Ibrahim RW, Safdar R, Nisar KS, et al. Thermal amelioration in heat transfer rate using Oldroyd-B model hybrid nanofluid by CNTs-based kerosene oil flow in solar collectors applications. Waves Random Complex Media. 2022;1–31.

[20] Shamshuddin MD, Animasaun IL, Salawu SO, Rao PS. Dynamics of ethylene glycol conveying MWCNTs and ethylene glycol conveying SWCNTs: Significant joule heating and thermal radiation. Numer Heat Transf Part Appl. 2023;1–20.

[21] Kiran Kumar T, Srinivasa Rao P, Shamshuddin Md. Effect of thermal radiation on nonDarcy hydromagnetic convective heat and mass transfer flow of a water–SWCNT's and MWCNT's nanofluids in a cylindrical annulus with thermo-diffusion and chemical reaction. Int J Mod Phys B. 2024 Jan;38(1):2450011.

[22] Hayat T, Haider F, Muhammad T, Ahmad B. Darcy–Forchheimer flow of carbon nanotubes due to a convectively heated rotating disk with homogeneous–heterogeneous reactions. J Therm Anal Calorim. 2019 Sep;137(6):1939–49.

[23] Rafique K, Mahmood Z, Khan U, Eldin SM, Alzubaidi AM. Mathematical analysis of radius and length of CNTs on flow of nanofluid over surface with variable viscosity and joule heating. Heliyon. 2023;9(7):e17673. [cited 2024 Mar 27]. https://www.cell.com/heliyon/pdf/S2405-8440(23)04881-8.pdf.

[24] Mahmood Z, Rafique K, Adnan, Khan U, Muhammad T, Hassan AM. MHD unsteady flow of carbon nanotubes over nonlinear radiative surface with anisotropic slip conditions: computational analysis of irreversibility for Yamada-Ota model. Eng Appl Comput Fluid Mech. 2024 Dec;18(1):2309139.

[25] Imtiaz M, Hayat T, Alsaedi A, Ahmad B. Convective flow of carbon nanotubes between rotating stretchable disks with thermal radiation effects. Int J Heat Mass Transf. 2016 Oct;101:948–57.

[26] Abbas N, Rehman KU, Shatanawi W, Abodayeh K. Mathematical model of temperature-dependent flow of power-law nanofluid over a variable stretching Riga sheet. Waves Random Complex Media. 2022;1–18.

[27] Mulinti VR, Lakshminarayana P. Influence of thermal radiation and viscous dissipation on MHD flow of UCM fluid over a porous stretching sheet with higher order chemical reaction. Spec Top Amp Rev Porous Media Int J. 2021;12.

[28] Khan M, Hashim, Hussain M, Azam M. Magnetohydrodynamic flow of Carreau fluid over a convectively heated surface in the presence of non-linear radiation. J Magn Magn Mater. 2016 Aug;412:63–8.

[29] Rehman KU, Malik AA, Malik MY, Ul Saba N. Mutual effects of thermal radiations and thermal stratification on tangent hyperbolic fluid flow yields by both cylindrical and flat surfaces. Case Stud Therm Eng. 2017 Sep;10:244–54.

[30] Vinodkumar Reddy M, Lakshminarayana P. Higher order chemical reaction and radiation effects on magnetohydrodynamic flow of a Maxwell nanofluid with Cattaneo–Christov heat flux model over a stretching sheet in a porous medium. J Fluids Eng. 2022;144(4):041204.

[31] Mushtaq A, Mustafa M, Hayat T, Alsaedi A. Nonlinear radiative heat transfer in the flow of nanofluid due to solar energy: A numerical study. J Taiwan Inst Chem Eng. 2014 Jul;45(4):1176–83.
[32] Rahman MM, Eltayeb IA. Radiative heat transfer in a hydromagnetic nanofluid past a non-linear stretching surface with convective boundary condition. Meccanica. 2013 Apr;48(3):601–15.
[33] Sheikholeslami M, Domiri Ganji D, Younus Javed M, Ellahi R. Effect of thermal radiation on magnetohydrodynamics nanofluid flow and heat transfer by means of two phase model. J Magn Magn Mater. 2015 Jan;374:36–43.
[34] Turkyilmazoglu M, Pop I. Heat and mass transfer of unsteady natural convection flow of some nanofluids past a vertical infinite flat plate with radiation effect. Int J Heat Mass Transf. 2013 Apr;59:167–71.
[35] Sakiadis BC. Boundary-layer behavior on continuous solid surfaces: II. The boundary layer on a continuous flat surface. AIChE J. 1961;7(2):221–5.
[36] Blasius H. Grenzschichten in Flüssigkeiten mit kleiner Reibung. Leipzig: Druck von B.G. Teubner; 1907. p. 46.
[37] Tsou FK, Sparrow EM, Goldstein RJ. Flow and heat transfer in the boundary layer on a continuous moving surface. Int J Heat Mass Transf. 1967 Feb;10(2):219–35.
[38] Tsai SY, Hsu TH. Thermal transport of a continuous moving plate in a non-Newtonian fluid. Comput Math Appl. 1995 Mar;29(6):99–108.
[39] Cortell Bataller R. Radiation effects in the Blasius flow. Appl Math Comput. 2008 Apr;198(1):333–8.
[40] Haile E, Shankar B. Boundary-layer flow of nanofluids over a moving surface in the presence of thermal radiation, viscous dissipation and chemical reaction. Appl Appl Math Int J AAM. 2015 Dec;10(2):21. https://digitalcommons.pvamu.edu/aam/vol10/iss2/21.
[41] Awan AU, Abid S, Abbas N. Theoretical study of unsteady oblique stagnation point based Jeffrey nanofluid flow over an oscillatory stretching sheet. Adv Mech Eng. 2020 Nov;12(11):1687814020971881.
[42] Bani-Fwaz MZ, Mahmood Z, Bilal M, EI-Zahhar AA, Khan I, Niazai S. Computational investigation of thermal process in radiated nanofluid modulation influenced by nanoparticles (Al2O3) and molecular (H2O) diameters. J Comput Des Eng. 2024;11(2):22–36.
[43] Mahmood Z, Rafique K, Khan U, Jubiar S, Awwad FA, Ismail EA. Investigation of entropy generation in the existence of heat generation and nanoparticle clustering on porous Riga plate during nanofluid flow. Mater Today Commun. 2024;38:108165.
[44] Khan U, Rafique K, Mahmood Z. Significance of unsteady rotating flow of nanofluid with nanoparticles aggregation and impacts of slip conditions and variable viscosity. Numer Heat Transf Part Appl. 2024 Jan;1–28.
[45] Alqahtani A, Rafique K, Mahmood Z, Al-Sinan B, Khan U, Hassan A. MHD rotating flow over a stretching surface: The role of viscosity and aggregation of nanoparticles. Heliyon. 2023 Oct;9:e21107.
[46] Al-Kouz W, Abderrahmane A, Shamshuddin MD, Younis O, Mohammed S, Bég OA, et al. Heat transfer and entropy generation analysis of water-Fe3O4/CNT hybrid magnetic nanofluid flow in a trapezoidal wavy enclosure containing porous media with the Galerkin finite element method. Eur Phys J Plus. 2021 Nov;136(11):1184.
[47] Masad JA, Nayfeh AH. Effects of suction and wall shaping on the fundamental parametric resonance in boundary layers. Phys Fluids Fluid Dyn. 1992 May;4(5):963–74.
[48] Rosali H, Ishak A, Pop I. Micropolar fluid flow towards a stretching/shrinking sheet in a porous medium with suction. Int Commun Heat Mass Transf. 2012 Jul;39(6):826–9.
[49] Pandey AK, Kumar M. Effect of viscous dissipation and suction/injection on MHD nanofluid flow over a wedge with porous medium and slip. Alex Eng J. 2016 Dec;55(4):3115–23.
[50] Aladdin NAL, Bachok N. Boundary layer flow and heat transfer of Al2O3-TiO2/water hybrid nanofluid over a permeable moving plate. Symmetry. 2020 Jun;12(7):1064.
[51] Bachok N, Ishak A, Pop I. Boundary layer flow over a moving surface in a nanofluid with suction or injection. Acta Mech Sin. 2012 Feb;28(1):34–40.
[52] Rafique K, Mahmood Z, Alqahtani A, Elsiddieg A, Khan U, Debani W, et al. Impacts of thermal radiation with nanoparticle aggregation and variable viscosity on unsteady bidirectional rotating stagnation point flow of nanofluid. Mater Today Commun. 2023 Jul;36:106735.
[53] Tadesse FB, Makinde OD, Enyadene LG. Hydromagnetic stagnation point flow of a magnetite ferrofluid past a convectively heated permeable stretching/shrinking sheet in a Darcy–Forchheimer porous medium. Sādhanā. 2021 Sep;46(3):115.